International Symposium
On Turbulence and Shear Flow
Phenomena (TSFP-9)
June 30 - July 3, 2015 *Melbourne, Australia*

ON THE EVALUATION OF NUMERICAL DISSIPATION RATE AND VISCOSITY IN A COMMERCIAL CFD CODE

G. Castiglioni and J. A. Domaradzki
Department of Aerospace and Mechanical Engineering
University of Southern California
Los Angeles, California 90089-1191
castigli@usc.edu, jad@usc.edu

ABSTRACT

Recently it has become increasingly clear that the role of a numerical dissipation, originating from the discretization of governing equations of fluid dynamics, rarely can be ignored while using explicit or implicit Large Eddy Simulations (LES). The numerical dissipation inhibits the predictive capabilities of LES whenever it is of the same order of magnitude or larger than the subgrid-scale (SGS) dissipation. The need to estimate the numerical dissipation is most pressing for low order methods employed by commercial CFD codes. Following the recent work of Schranner *et al.* (2015) the equations and procedure for estimating the numerical dissipation rate and the numerical viscosity in a commercial code will be presented. The method allows to compute the numerical dissipation rate and numerical viscosity in the physical space for arbitrary sub-domains in a self-consistent way, using only information provided by the code in question. It is the first time this analysis has been applied to low-order incompressible and compressible solvers. The procedure is tested for a three-dimensional Taylor-Green vortex flow and compared with benchmark results obtained using an accurate, incompressible spectral solver.

INTRODUCTION

Direct Numerical Simulations (DNS) of turbulent flows are excessively computationally expensive for complex geometries and/or high Reynolds number flows due to the wide separation of physical scales that need to be resolved. A relatively successful way to reproduce the dynamics of Navier-Stokes (N-S) equations while reducing the number of degrees of freedom is the Large Eddy Simulations (LES) approach. In LES the number of degrees of freedom is reduced by means of a spatial filter that suppresses the effects of small scales at the cost of introducing subgrid scale (SGS) unknowns (i.e. for the incompressible N-S the SGS stress tensor) which must be explicitly modeled (Pope, 2000; Sagaut, 2006; Garnier *et al.*, 2009). An alternative approach is to use the numerical dissipation coming from the discretization of the N-S equations as an implicit LES (ILES) model. The strategy of using the truncation error as implicit model dubbed monotonically integrated LES (MILES) originated with the idea of Boris *et al.* (1992) and is reviewed by Grinstein *et al.* (2007). MILES approach has been controversial and as such it has been subject of rigorous investigations (Garnier *et al.*, 1999; Domaradzki *et al.*, 2003). These studies have not been particularly encouraging. Even when MILES appears to reproduce qualitatively the dynamics of N-S equations a more in depth, quantitative investigation has shown that this is not the case. Broadly speaking in these studies have been presented two scenarios. The first one (Garnier *et al.*, 1999) is that the numerical dissipation is excessive with respect to the correct SGS dissipation leading to poor results both in ILES and explicit LES (ELES) configuration. The other option is that the scheme is under-dissipative (with respect to the correct SGS dissipation) leading to good results for short time integrations and poor results for long time integrations due to accumulation of energy in the high wave numbers (Domaradzki *et al.*, 2003). The latter case can potentially be adjusted either by filtering or with the addition of an explicit SGS model. Both situations shows a fundamental deficiency of the MILES approach: there is no mechanisms embedded in the numerics to ensure correct amount of SGS dissipation. This observation, that can appear crudely obvious, suggested that rather than calling this approach ILES it should be called under-resolved DNS (UDNS) furthermore the term ILES should be reserved for schemes that are designed in such a way that the discretization error provides the correct amount of SGS dissipation. An example of such schemes is the adaptive local deconvolution method (ALDM) of Hickel *et al.* (2006). In the ALDM the discretization is based on a solution-adaptive deconvolution operator which allows to control the truncation error so that the numerical viscosity can match the theoretical values for isotropic turbulence. Early ELES studies pointed out that low-order models are not suitable in the ELES framework as the interaction between numerical dissipation and the SGS dissipation (Kravchenko & Moin, 1997) would negatively affect the results, while for high-order/spectral methods the leading source of error is aliasing of the non-linear term. Recently it has been shown that at very coarse resolutions even formally high-order methods can suffer from the interaction between numerical dissipation and SGS dissipation making the addition of an ELES model detrimental to the performance of the code (Cadieux *et al.*, 2014). On the other hand UDNS simulations (often improperly called ILES) are becoming more and more popular. The reason for this trend and the attractiveness of the approach are due to several reasons: its simplicity, the lack of a universal explicit SGS model and a qualitative behavior that mimics the dynamics of N-S equations. Furthermore UDNS simulation often are validated with experi-

mental results which suffer from high degree of uncertainty. Recently the need of quantifying the numerical dissipation has been addressed by Schranner *et al.* (2015) who developed a new methodology that allows the quantification of numerical dissipation in a self consistent way, using only information provided by the code analyzed. Through the quantification of numerical dissipation, the tool proposed by Schranner *et al.* (2015) is a rigorous method to judge a posteriori the quality of a given simulation allowing for an impartial assessment of the impact of the numerical dissipation. Here we apply this methodology for the first time to a low-order incompressible and compressible solver, validating the method with the goal to extend it to more realistic configurations.

EQUATIONS AND METHOD

Analytical Form

Transport energy equation for compressible Navier-Stokes (N-S) is

$$\frac{\partial \rho e}{\partial t} + \frac{\partial}{\partial x_j}\left[(\rho e + p)\, u_j\right] = \frac{\partial u_i \tau_{ij}}{\partial x_j} - \frac{\partial q_j}{\partial x_j}, \qquad (1)$$

where u_i are the components of the velocity vector, p the pressure, ρ the density and e the total energy per unit mass. The constitutive relation between stress and strain rate for a Newtonian fluid is

$$\tau_{ij} = \mu\left[\left(\frac{\partial u_i}{\partial x_j} + \frac{\partial u_j}{\partial x_i}\right) - \frac{2}{3}\frac{\partial u_k}{\partial x_k}\delta_{ij}\right], \qquad (2)$$

the heat flux q_i is defined as

$$q_i = -k\frac{\partial T}{\partial x_i}, \qquad (3)$$

where μ is the dynamic viscosity, k is the thermal conductivity, and T is the temperature. The definition of total energy is

$$e = e^{in} + e^{kin}, \qquad (4)$$

where e^{in} is the specific energy per unit mass and $e^{kin} = \frac{1}{2}u_i u_i$ the kinetic energy. Following the procedure of Schranner *et al.* (2015) the transport equation, Eq. (1), can be separated into the contribution of internal energy

$$\frac{\partial \rho e^{in}}{\partial t} + \frac{\partial \rho e^{in} u_j}{\partial x_j} = -p\frac{\partial u_j}{\partial x_j} + \tau_{ij}\frac{\partial u_i}{\partial x_j} - \frac{\partial q_j}{\partial x_j}, \qquad (5)$$

and kinetic energy

$$\frac{\partial \rho e^{kin}}{\partial t} + \frac{\partial \rho e^{kin} u_j}{\partial x_j} = -u_j\frac{\partial p}{\partial x_j} + u_i\frac{\partial \tau_{ij}}{\partial x_j}. \qquad (6)$$

After some manipulations the integral form of Eq. (6) can be written as

$$\begin{aligned}&\frac{\partial}{\partial t}\int_V \rho e^{kin} dV + \int_A \left(\rho e^{kin} u_j + u_j p - u_i \tau_{ij}\right) n_j dA \\ &+ \int_V \left(-p\frac{\partial u_j}{\partial x_j} + \tau_{ij}\frac{\partial u_i}{\partial x_j}\right) dV = \\ &\frac{\partial}{\partial t}E^{kin} + F^{kin} + F^{ac} - F^{vis} - W^p + \varepsilon^{vis} = 0, \end{aligned} \qquad (7)$$

where F^{kin}, F^{ac}, F^{vis} are the kinetic energy, acoustic and viscous fluxes, n_j the outward unit vector normal to the surface A, W^p the work due to pressure and ε^{vis} the viscous dissipation. Notice that in the incompressible limit $W^p = 0$ as $\partial u_j/\partial x_j = 0$.

We can define a dissipation function ε as

$$\varepsilon = \int_V \frac{1}{\nu}\tau_{ij}\frac{\partial u_i}{\partial x_j} dV, \qquad (8)$$

therefore $\varepsilon\nu = \varepsilon^{vis}$, where ν is the kinematic viscosity ($\nu = \mu/\rho$). Note that the above equation is exact only if $\nu = const$ in V.

Discretized Form

If we assume a FV spatial discretization and generic discretization in time then the Eq. (7) is contaminated by the truncation and aliasing errors so we can define a local residual

$$-\varepsilon^n_{(m)} = \frac{\Delta E^{kin}_{(m)}}{\Delta t} + F^{kin}_{(m)} + F^{ac}_{(m)} - F^{vis}_{(m)} - W^p_{(m)} + \varepsilon^{vis}_{(m)}, \qquad (9)$$

where the subscript $[\ \ ]_{(m)}$ refers to the mth control volume. We call the residual ε^n numerical dissipation rate because it has been shown that if integrated over a sufficiently large control volume it has a predominantly dissipative character (Schranner *et al.*, 2015; Domaradzki & Radhakrishnan, 2005). Following this definition we can recover the numerical kinematic viscosity as

$$\nu^n_{(m)} = \frac{\varepsilon^n_{(m)}}{\varepsilon_{(m)}}. \qquad (10)$$

We can extend the above definitions to a sub-domain or to the entire computational domain

$$\varepsilon^n_{sub} = \sum_m^M \varepsilon^n_{(m)} \quad ; \quad \nu^n_{sub} = \frac{\varepsilon^n_{sub}}{\varepsilon_{sub}}, \qquad (11)$$

where M is total number of adjacent cells of a given subdomain.

PROCEDURE

This is a posteriori procedure, all quantities come from the computed flow field. For the time discretization a

second-order three-points finite difference formula is used. Kinetic fluxes are calculated as follow

$$F^{kin}_{(m)} = \left(\sum_r (\rho e^{kin} u_j n_j)_{(r)} \Delta A_{(r)} \right)_{(m)}, \tag{12}$$

where subscript $[\quad]_{(r)}$ represents the sum over the rth face of the mth control volume and $\Delta A_{(r)}$ is the area of the rth face. The other fluxes are computed in similar fashion. Volume terms are calculated as (for example the kinetic energy)

$$E^{kin}_{(m)} = \left(\frac{1}{2} \rho u_i u_i \right)_{(m)} \Delta V_{(m)}, \tag{13}$$

where $\Delta V_{(m)}$ is the volume of the mth control volume. In the infinite Re number limit the viscous terms in Eq. (9) are dropped. In the incompressible limit ($Ma < 0.3$) the work due to pressure should be zero, this is not the case if the flow field is not divergence free (as it can happen with low-order incompressible schemes). Also note that if we take a periodic box the contribution of flux terms cancels out.

NUMERICAL METHOD

Star-CCM+ solves either the incompressible or compressible three-dimensional integral Navier-Stokes equations in conservative form. The equations are solved in a preconditioned dimensional form on an unstructured grid (CD-Adapco, 2013). The time is advanced through a dual time-stepping implicit scheme. The incompressible solver uses a Rhie-Chow pressure-velocity coupling and a SIMPLE algorithm, while the for the compressible solver the inviscid fluxes are evaluated by using the Weiss-Smith preconditioned Roe's flux-difference splitting scheme. Both schemes are formally at best second order accurate. The viscous fluxes are evaluated by a standard central difference scheme.

VALIDATION

This is the same case which was analyzed previously to validate the procedure applied to a research code INCA that implements the ALDM method as an implicit LES model (Schranner *et al.*, 2015; Hickel *et al.*, 2006). The Taylor Green Vortex (TGV) problem is originally described in Taylor & Green (1937). The initial conditions, following (Shu *et al.*, 2005), are

$$u = u_0 \left[sin(x) cos(y) cos(z) \right], \tag{14}$$

$$v = -u_0 \left[cos(x) sin(y) cos(z) \right], \tag{15}$$

$$w = 0, \tag{16}$$

$$\rho = \rho_0, \tag{17}$$

$$p = p_0 + \frac{\rho_0}{16} \left[(cos(2x) + cos(2y))(cos(2z) + 2) - 2 \right], \tag{18}$$

where subscript $[\quad]_0$ indicates reference quantities. The initial flow field is let to evolve for 10 non-dimensional time units. The time unit is $T = l_0/u_0$ where $l_0 = 1$ is the reference length. The time step is kept constant as $\Delta t = T/50$. Star-CCM+ solves the dimensional form of the N-S. Under ideal gas assumption, to obtain the same initial condition as in Schranner *et al.* (2015) and Hickel *et al.* (2006) we need to pick the following reference values: $u_0 = Ma\sqrt{\gamma p_0/\rho_0}$ and $\rho_0 = p_0/(R\,T_0)$. The reference pressure is $p_0 = 101325\ Pa$, the Mach number $Ma = 0.0845$, the heat capacity ratio $\gamma = 1.4$, the reference temperature $T_0 = 300\ K$ and the specific gas constant $R = 287.02\ J/(kg\ K)$. Even though the code solves the dimensional N-S equations, all results will be presented in non-dimensional form. Unless stated otherwise the resolution for all simulations is of 64 cells per spatial direction for a cube with sides that are 2π long and that has periodic boundary conditions. Initially all simulations are run with the incompressible solver for a direct comparison with the work of Schranner *et al.* (2015), afterwards selected cases are run with the compressible solver.

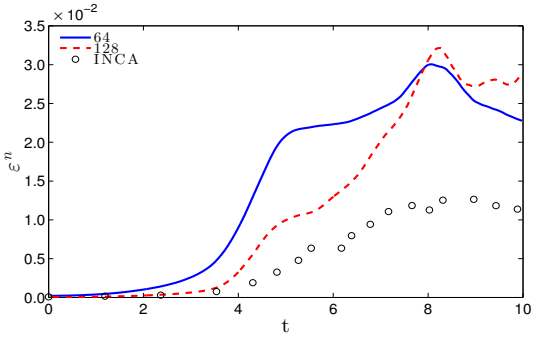

Figure 1. Time-evolution of numerical dissipation rate ε^n_{tot}, $Re = \infty$. Star-CCM+ with 64^3 cells (blue line), Star-CCM+ with 128^3 cells (red dashed line) and INCA from Schranner *et al.* (2015) (black circles).

Full periodic domain

For the first test case we use as a control volume the whole domain so that we can calculate the total numerical dissipation rate without flux terms. For $Re = \infty$ we show ε^n_{tot} plotted against time in Fig. 1. The numerical dissipation rate is quite high, it is around three times as much as in Schranner *et al.* (2015) throughout the temporal domain. To make sure that the ε^n_{tot} is calculated properly this case has been repeated with 128 cells per spatial direction. This case can also be seen in Fig. 1. We can observe that for the laminar part of the simulation ($t < 3.5$) there is indeed fairly good agreement with the reference results. Enstrophy ($\Omega = 1/2 \int_V \omega_i \omega_i dV$, where ω_i are the component of the vorticity vector) is often used in TGV simulations as a metric to judge the degree of resolution. It is hypothesized that for the inviscid TGV problem enstrophy should increase to infinity at the non-dimensional time $t \approx 5$ (Shu *et al.*, 2005). The resolution of this singularity is a common metric to evaluate a given scheme/resolution for a TGV simulation. In Fig. 2 we can see that for our current simulation we fall in between the behavior of a spectral scheme, which has very little numerical dissipation and a fifth-order WENO scheme which has substantial numerical dissipation, with Star-CCM+ closer to the latter. This is expected since the current scheme is formally at best second order, therefore quite dissipative. The result for the 128^3 case is also included. While this is not a fair comparison neither with the spectral nor the WENO schemes used with the 64^3 resolu-

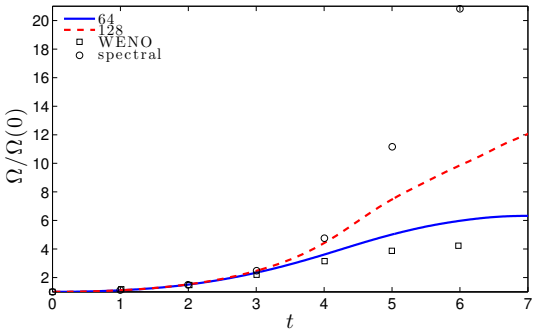

Figure 2. Time-evolution of normalized enstrophy $\Omega(t)/\Omega(0)$, $Re = \infty$. Star-CCM+ with 64^3 cells (blue line), with 128^3 cells (red dashed line), WENO (black squares) and spectral (black circles) from Shu *et al.* (2005).

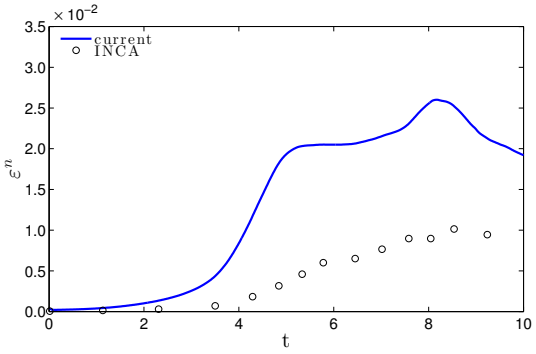

Figure 3. Time-evolution of numerical dissipation rate ε^n_{tot}, $Re = 3000$. Star-CCM+ (blue line) and INCA from Schranner *et al.* (2015) (black circles).

tion, it is still a useful way to show that the numerical dissipation of the current scheme approaches the spectral numerical dissipation when the resolution increases. For the same configuration, as in the reference paper, a sweep of Reynolds number has been ran ($Re = \infty$, 3000, 1600, 800, 400, 200, and 100). We can see ε^n_{tot} plotted against time in Figures $3-4$ for two of those cases. The general trend is the same as in the infinite Reynolds number case, and the peak is about 2.5 times the peak in the reference study. In Fig. 5 we show a full sweep of Reynolds numbers to better appreciate the behavior of the numerical dissipation rate as a function of the Reynolds number.

Sub-domains

As test cases we choose some of the sub-domains used in Schranner *et al.* (2015). The first cubic sub-domain used in the reference was an octant of the domain. Due to symmetries of the TGV problem this case is only useful to check that all fluxes cancel out. The second test case simulated is the cubic sub-domain one (CSD1) which consists of cells 10 through 56 in all spatial directions. The results for the infinite Reynolds number case are shown in Fig. 6. Here and in the following Figures terms of the kinetic energy balance are plotted with a negative sign in order to sum up to ε^n. All the current results are plotted against the results from the reference paper and also plotted are the various terms

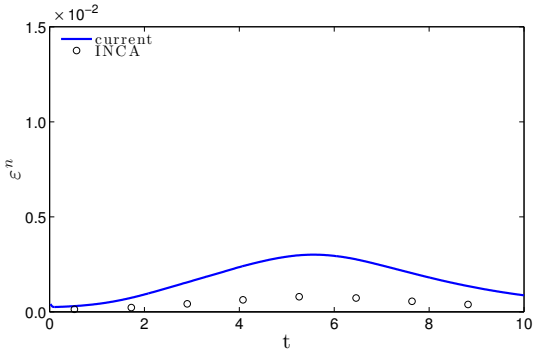

Figure 4. Time-evolution of numerical dissipation rate ε^n_{tot}, $Re = 100$. Star-CCM+ (blue line) and INCA from Schranner *et al.* (2015) (black circles).

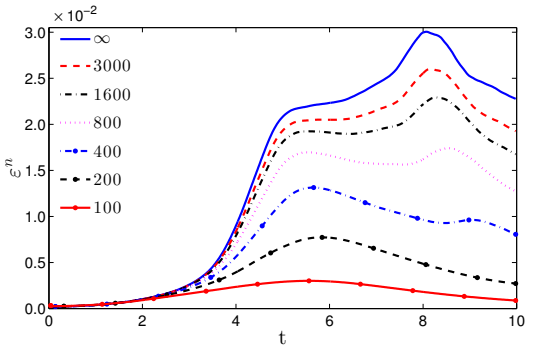

Figure 5. Time-evolution of numerical dissipation rate ε^n_{tot}. $Re = \infty$ (blue line), $Re = 3000$ (red dashed line), $Re = 1600$ (black dash-dotted line), $Re = 800$ (magenta dotted line), $Re = 400$ (solid blue line with markers), $Re = 200$ (red dashed line with markers), and $Re = 100$ (black dash-dotted line with markers) .

that contribute to the numerical dissipation rate. We can see that we recover the same trend observed in the infinite Reynolds number case with the full periodic box, i.e. for the laminar part of the simulation the results agree with the spectral reference while the peak in the turbulent part of the simulation is about 3 times as high. In Fig. 6 we can see a noisy oscillatory behavior in the acoustic flux term and the work due to pressure. These oscillations are out of phase and cancel each other out. We speculate that this is an unphysical energy exchange between the two terms due to the fact that incompressibility is not strictly enforced. For the finite Re cases we see the same trend observed for the periodic box cases. A sweep of Re has been performed, here we report only two cases: $Re = 3000, 100$ (see Figures $7-8$). To better visualize the additional dissipation provided by the scheme with respect to the physical dissipation we have plotted the molecular viscosity ν together with the total effective viscosity $\nu + \nu^n$, i.e. a sum of the numerical and the physical viscosity, for the $Re = 3000$ case (see Fig. 9).

The only non-cubic sub-domain considered here is the NCSD2 from reference Schranner *et al.* (2015), i.e. for the x-direction cells 8 to 23 and for the y and z-direction cells 1 to 31. This sub-domain is not chosen randomly, it was selected because this is the region within the octant with

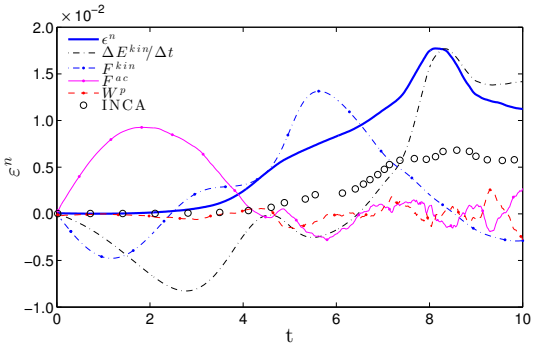

Figure 6. Time-evolution of numerical dissipation rate ε^n_{sub}, $Re = \infty$, sub-volume CSD1. Numerical dissipation rate ε^n_{sub} (blue line), rate of change of kinetic energy $-\Delta E^{kin}_{sub}/\Delta t$ (black dot-dashed line), kinetic energy flux $-F^{kin}_{sub}$ (blue dot-dashed line with markers), acoustic flux $-F^{ac}_{sub}$ (magenta dotted line) and INCA from Schranner *et al.* (2015) (black circles).

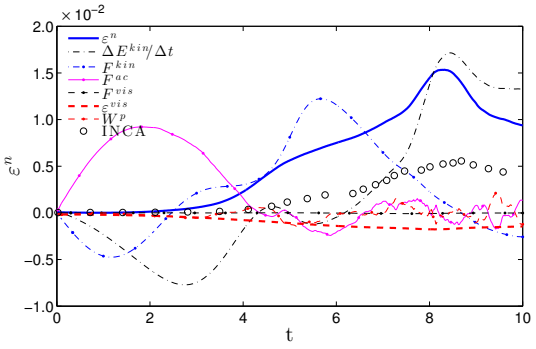

Figure 7. Time-evolution of numerical dissipation rate ε^n_{sub}, $Re = 3000$, sub-volume CSD1. Numerical dissipation rate ε^n_{sub} (blue line), rate of change of kinetic energy $-\Delta E^{kin}_{sub}/\Delta t$ (black dot-dashed line), kinetic energy flux $-F^{kin}_{sub}$ (blue dot-dashed line with markers), acoustic flux $-F^{ac}_{sub}$ (magenta solid line with markers), viscous flux F^{vis}_{sub} (black dashed line with markers) viscous dissipation rate $-\varepsilon^{vis}_{sub}$ (red dashed line) and INCA from Schranner *et al.* (2015) (black circles).

non-negligible numerical dissipation within an octant. The results for the subdomain NCSD2 are shown in Fig. 10.

Surface versus Volume Integrals

For certain incompressible solvers pressure can be defined up to a constant without changing the dynamics of the flow field since only the gradient of pressure appears directly in the momentum equations. For this reason simply adding W^p_{sub} to the energy balance can potentially lead to wrong estimates of the numerical dissipation rate. One way to check for consistency of the results is to recast the pressure terms as $F^{ac}_{(m)} - W^p_{(m)} = pt_{(m)}$, where $pt_{(m)}$ is the numerical form of the pressure transport term defined as $pt_{(m)} = \left(u_j \frac{\partial p}{\partial x_j}\right)_{(m)} \Delta V_{(m)}$. As can be seen comparing Figures 6 and 11 the two methods are equivalent. Other surface

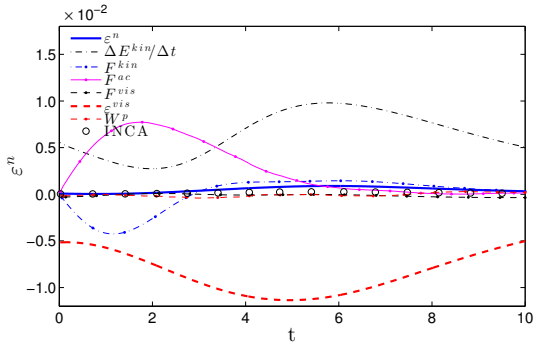

Figure 8. Time-evolution of numerical dissipation rate ε^n_{sub}, $Re = 100$, sub-volume CSD1. Numerical dissipation rate ε^n_{sub} (blue line), rate of change of kinetic energy $-\Delta E^{kin}_{sub}/\Delta t$ (black dot-dashed line), kinetic energy flux $-F^{kin}_{sub}$ (blue dot-dashed line with markers), acoustic flux $-F^{ac}_{sub}$ (magenta solid line with markers), viscous flux F^{vis}_{sub} (black dashed line with markers) viscous dissipation rate $-\varepsilon^{vis}_{sub}$ (red dashed line) and INCA from Schranner *et al.* (2015) (black circles).

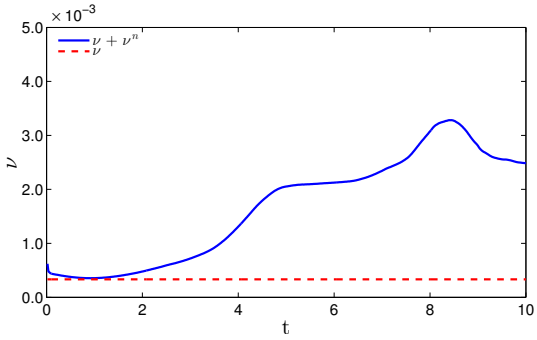

Figure 9. Time-evolution of physical and numerical viscosity, $Re = 3000$, sub-volume CSD1. Total viscosity $\nu + \nu^n$ (blue line), physical viscosity ν (red dashed line).

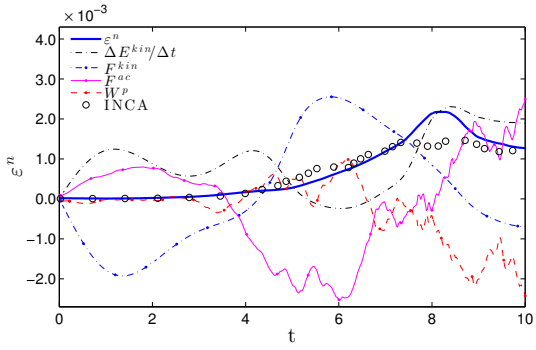

Figure 10. Time-evolution of numerical dissipation rate ε^n_{sub}, $Re = \infty$, sub-volume NCSD2, including work due to pressure. Numerical dissipation rate ε^n_{sub} (blue line), rate of change of kinetic energy $-\Delta E^{kin}_{sub}/\Delta t$ (black dot-dashed line), kinetic energy flux $-F^{kin}_{sub}$ (blue dot-dashed line with markers), acoustic flux $-F^{ac}_{sub}$ (magenta solid line with markers), W^p_{sub} (red dashed line with markers) and INCA from Schranner *et al.* (2015) (black circles).

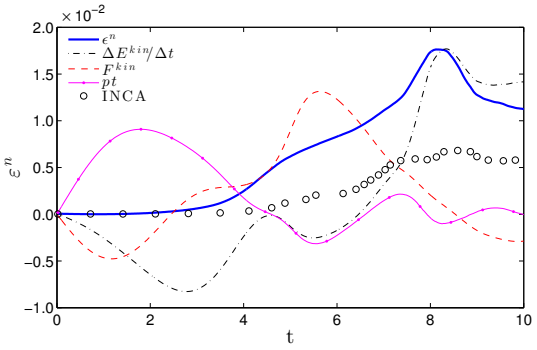

Figure 11. Time-evolution of numerical dissipation rate ε^n_{sub}, $Re = \infty$, sub-volume CSD1 with pressure gradient transport term. Numerical dissipation rate ε^n_{sub} (blue line), rate of change of kinetic energy $-\Delta E^{kin}_{sub}/\Delta t$ (black dot-dashed line), kinetic energy flux $-F^{kin}_{sub}$ (red dashed line), acoustic flux $-F^{ac}_{sub}$ (magenta dotted line), $-pt_{sub}$ (magenta solid line with markers) and INCA from Schranner *et al.* (2015) (black circles).

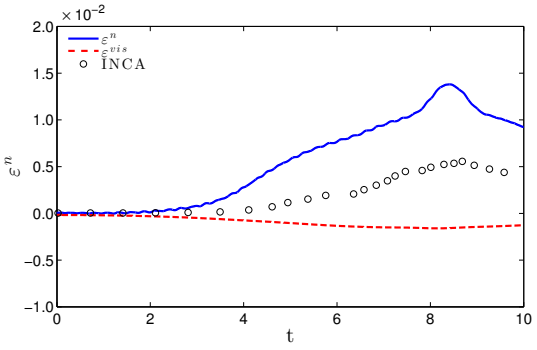

Figure 12. Time-evolution of numerical dissipation rate ε^n_{sub} for a compressible solver, $Ma = 0.0845$, $Re = 3000$, sub-volume CSD1. Numerical dissipation rate ε^n_{sub} (blue line), viscous dissipation rate $-\varepsilon^{vis}_{sub}$ (red dashed line) and INCA from Schranner *et al.* (2015) (black circles).

terms have been calculated as volume terms with similar conclusions; there seem to be negligible differences in calculating the quantities in the kinetic energy balance as either volume or surface integrals.

Effects of Compressibility

All simulations so far have been performed with an incompressible solver to have a one to one comparison with the results available in literature. Due to convergence issues for the compressible case the time step has been reduced to $\Delta t = T/500$. For the CSD1 sub-domain all Reynolds number cases have been run for a complete comparison with the incompressible simulations. Here we report only the case for $Re = 3000$, see Fig. 12 where the physical and the numerical dissipation rates are plotted. We find a good agreement with the incompressible solver at all Reynolds numbers.

DISCUSSION AND CONCLUSIONS

Even lacking a direct validation through an external spectral code as in the reference paper of Schranner *et al.* (2015) the methods applied to a low-order incompressible and compressible schemes compares well to the available reference data and it is self consistent. It should be noted that for low-order schemes the work due to pressure, even though should be zero, might not be negligible. The extension to a compressible solver, at least at low Mach numbers, is straightforward. From our results it seems to not matter if terms in the discrete kinetic energy balance, Eq. (9), are calculated as fluxes or as volume terms. The method seems self consistent and robust as all our results are in qualitative agreement with the results of Schranner *et al.* (2015). Therefore we conclude that the method works well for low-order schemes and that it is ready to be applied to more realistic flow geometries.

REFERENCES

Boris, J.P., Grinstein, F.F., Oran, E.S. & Kolbe, R.L. 1992 New insights into large eddy simulation. *Fluid Dyn. Res.* **10**, 199–228.

Cadieux, F., Domaradzki, J. A., Sayadi, T. & Bose, T. 2014 DNS and LES of laminar separation bubbles at moderate Reynolds numbers. *ASME J. Fluids Eng.* **136**, 061102.

CD-Adapco 2013 Star-CCM+ manual. Version 8.02.

Domaradzki, J.A. & Radhakrishnan, S. 2005 Eddy viscosities in implicit large eddy simulations of decaying high Reynolds number turbulence with and without rotation. *Fluid Dyn. Res.* **36**, 385–406.

Domaradzki, J. A., Xiao, Z. & Smolarkiewicz, P. K. 2003 Effective eddy viscosities in implicit large eddy simulations of turbulent flows. *Phys. Fluids* **15** (12), 3890–3893.

Garnier, E., Adams, N. & Sagaut, P. 2009 *Large eddy simulation for compressible flows*. Springer.

Garnier, E., Mossi, M., Sagaut, P., Comte, P. & Deville, M. 1999 On the use of shock-capturing schemes for large-eddy simulation. *J. Comp. Phys.* **153** (2), 273–311.

Grinstein, F., Margolin, L. & Rider, W. 2007 *Implicit Large Eddy Simulation: Computing Turbulent Flow*. Cambridge University Press.

Hickel, S., Adams, N.A. & Domaradzki, J.A. 2006 An adaptive local deconvolution method for implicit LES. *J. Comp. Phys.* **213**, 413–436.

Kravchenko, A.G. & Moin, P. 1997 On the effect of numerical errors in large eddy simulations of turbulent flows. *J. Comp. Phys.* **131** (2), 310–322.

Pope, S. B. 2000 *Turbulent flows*. Cambridge University Press.

Sagaut, P. 2006 *Large eddy simulation for incompressible flows: an introduction*, 3rd edn. Springer.

Schranner, F.S., Domaradzki, J.A., Hickel, S. & Adams, N.A. 2015 Assessing the numerical dissipation rate and viscosity in numerical simulations of fluid flows. *Comp. & Fluids* **114**, 84–97.

Shu, C.-W., Don, W.-S., Gottlieb, D., Schilling, O. & Jameson, L. 2005 Numerical convergence study of nearly incompressible, inviscid TaylorGreen vortex flow. *J. Sci. Comp.* **24** (1).

Taylor, G.I. & Green, A.E. 1937 Mechanism of the production of small eddies from large ones. *Proc. R. Soc. Lond. A* **158** (895), 499–521.